

COLOR GRADIENTS IN EARLY-TYPE GALAXIES IN CLUSTERS AT REDSHIFT 0.37–0.56

NAOYUKI TAMURA AND KOUJI OHTA

Department of Astronomy, Faculty of Science, Kyoto University, Kyoto 606-8502, Japan; tamura@kusastro.kyoto-u.ac.jp

Received 2000 February 18; accepted 2000 March 11

ABSTRACT

Color gradients in elliptical galaxies in distant clusters ($z = 0.37\text{--}0.56$) are examined by using the archival deep imaging data of the Wide Field Planetary Camera 2 on board the *Hubble Space Telescope* (*HST*). Obtained color gradients are compared with the two model gradients to examine the origin of the color gradients. In one model, a color gradient is assumed to be caused by a metallicity gradient of stellar populations, while in the other one, it is caused by an age gradient. Both of these model color gradients reproduce the average color gradient seen in nearby elliptical galaxies, but predict significantly different gradients at redshift larger than ~ 0.3 . Comparison of the observed gradients and the model gradients favors the metallicity gradient much more than the age gradient as the primary origin of color gradients in elliptical galaxies in clusters. The same conclusion has been obtained for field elliptical galaxies by using those at redshift 0.1–1.0 in the Hubble Deep Field North by Tamura et al. Thus, it is also suggested that the primary origin of the color gradients in elliptical galaxies does not depend on galaxy environment.

Key words: galaxies: elliptical and lenticular, cD — galaxies: evolution — galaxies: formation

1. INTRODUCTION

It has been known that nearby elliptical galaxies have color gradients; colors in an elliptical galaxy gradually become bluer with increasing radius (e.g., Vader et al. 1988; Franx, Illingworth, & Heckman 1989; Peletier et al. 1990a; Peletier, Valentijn, & Jameson 1990b; Goudfrooij et al. 1994; Michard 1999). Since many elliptical galaxies show radial gradients in metal absorption-line strengths such as Mg_2 , Fe_1 (5270 Å), and Fe_2 (5335 Å) (e.g., Carollo, Danziger, & Buson 1993; Davies, Sadler, & Peletier 1993; Gonzalez 1993; Kobayashi & Arimoto 1999), the origin of the color gradients has been naively interpreted to be in the metallicity gradients.

However, such an interpretation for the origin of the color gradient is premature, because both the metallicity gradient and the age gradient in stellar populations can cause the same color gradient, and we cannot distinguish the cause for the gradient. This is called the age-metallicity degeneracy and was originally pointed out by Worthey, Trager, & Faber (1996) in terms of the origin of the color-magnitude relation of nearby elliptical galaxies (see also Arimoto 1996). To break this degeneracy and to know the primary origin of the color gradients in elliptical galaxies, comparing the observed color gradients in distant elliptical galaxies with predicted model gradients caused by either the metallicity gradient or the age gradient is a very effective approach, as it was successful for examining the origin of the color-magnitude (C-M) relation (Kodama & Arimoto 1997). Tamura et al. (2000, hereafter Paper I) constructed two models, both of which reproduce typical color gradients of elliptical galaxies at $z = 0$ using a population synthesis model. In one model, the mean metallicity of the stellar population decreases with increasing radius at a fixed old mean age, while in the other one, the mean age decreases with a radius at a fixed mean metallicity. These models were then evolved backward in time. The evolution of the color gradients thus predicted are compared with the observed ones in distant ($z \sim 0.1\text{--}1.0$) elliptical galaxies sampled from the Hubble Deep Field North (HDF-N; Williams et al. 1996). As a result, Paper I found that the metal-

licity gradient is the primary origin of color gradients and the age-gradient model cannot reproduce the observed gradient at such redshift.

The elliptical galaxies in the HDF-N, however, are only those in the field environment. It has never been obvious that elliptical galaxies in clusters evolve similarly to those in the field. In rich clusters, it has been found that the color-magnitude relation holds even at about $z \sim 1$ (e.g., Stanford, Eisenhardt, & Dickinson 1998), and these observational results seem to favor the classical monolithic-collapse scenario associated with the galactic wind and high z formation (e.g., $z > 3$) of elliptical galaxies (e.g., Kodama et al. 1998a). However, this kind of evolution has not been established for elliptical galaxies in lower density environments (cf. Kodama, Bower, & Bell 1998b). Some studies predict either theoretically or observationally that field elliptical galaxies formed by recent (at $z \leq 1$) merging processes (e.g., Baugh, Cole, & Frenk 1996; Barger et al. 1999). An internal structure of a galaxy, such as the metallicity gradient or the age gradient, must depend on its formation process. If cluster elliptical galaxies have formation histories different from those for field elliptical galaxies, their internal structures, and thus the origin of the color gradients, may not be the same, or some environmental effects on color gradients may exist. Thus, for cluster elliptical galaxies the same approach is needed to clarify the origin of their color gradients.

It is noted that dust extinction in elliptical galaxies may also have some effects on the color gradients (Goudfrooij & de Jong 1995; Wise & Silva 1996; Silva & Wise 1996). However, about half the detection toward elliptical galaxies in the far-infrared with IRAS have threshold about 3σ , and confirmation is needed to be definitive (Bregman et al. 1998). In addition, the spatial distribution of dust in an elliptical galaxy, as well as dust mass that could affect a color gradient, is not established yet. These are still open problems and will be examined in detail in our forthcoming papers. Therefore, in this paper we have chosen to focus only on age and metallicity effects.

This paper is organized as follows: The sample selection

and data analysis of elliptical galaxies are described in § 2. Histograms of color gradients are presented in § 3, together with the representative color profiles of the sample elliptical galaxies. Discussion is presented in § 4. The cosmological parameters adopted throughout this paper are the same as those in Paper I: $H_0 = 50 \text{ km s}^{-1} \text{ Mpc}^{-1}$, $\Omega_0 = 0.2$, and $\Lambda = 0$.

2. DATA AND SAMPLE SELECTION

To examine color gradients in elliptical galaxies in distant clusters, deep imaging data with high angular resolution in more than two bands are necessary. Thus, we choose to use the archival data taken with the Wide Field Planetary Camera 2 (WFPC2) on board the *Hubble Space Telescope* (*HST*). Smail et al. (1997) obtained deep imaging data of 11 distant rich clusters at redshifts from 0.37 to 0.56, most of which have exposure times longer than 10,000 s, to examine their morphology in detail and presented catalogs of the detected objects. In this paper, their reduced imaging data, available at their Web site,¹ are used. From these data, we select six clusters whose images were taken in two bands to obtain galaxy colors. Clusters with their basic properties taken from Smail et al. (1997) are listed in Table 1. Among these clusters, CL 0024+16, CL 0016+16, and CL 0054–27 are classified as high-concentration clusters and CL 0939+47 and CL 0412–65 are low-concentration clusters (Dressler et al. 1997). For A370 and CL 0939+47, the images of their outer fields were taken. Therefore environmental effects on color gradients may be examined.

Early-type galaxies (E, E/S0, S0/E) in these clusters are sampled based on the catalog by Smail et al. (1997). Since our main interest is to examine their color gradients, a high signal-to-noise ratio (S/N) is required, and thus galaxies brighter than the apparent 21 mag in the I_{814} band are selected in all the sample clusters. This apparent magnitude roughly corresponds to the absolute magnitude -20 in the V band. Our sample galaxies are listed in Tables 2–7 with their basic parameters, most of which are taken from Smail et al. (1997). In each cluster, the sample galaxies form the

tight C-M relations as shown in Figure 1, though the relations in A370, CL 0939+47, and CL 0412–65 are somewhat loose. Since CL 0939+47 and CL 0412–65 are classified as low-concentration clusters and the outer regions of the clusters were imaged for A370 and CL 0939+47, some environmental effects on the C-M relations might be seen. However, a discussion for this subject is beyond our scope in this paper. In the figure, a square in a circle indicates that the object was removed from the following analysis because its color gradient could not be derived accurately enough to apply our discussion, because of a low S/N or because of a position close to an edge of the image.

3. PROFILES AND COLOR GRADIENTS

In deriving color profiles of the sample galaxies, we should take care of positional coincidences of a blue image and a red image and differences in the size of the point-spread functions (PSFs) for the two images. (One pixel corresponds to $0''.10$ for the Wide Field Cameras and $0''.046$ for the Planetary Camera.) Positional displacement of a blue image from a red one causes spurious asymmetry in the color distribution in a galaxy and has a serious effect on the color gradient. We examined the centroids of the sample galaxies in both blue and red images and corrected the displacement if a systematic shift between the two images in each cluster was found. The sizes of the PSFs should be also estimated and adjusted for blue and red images. We simulated the PSF at each position of a sample galaxy in each band by using Tiny Tim version 4.4 (Krist 1995; Krist & Hook 1997) and corrected the difference in size for the two images, which was estimated by fitting a Gaussian to the PSFs. Sky value was determined by “mode” in an annulus with inner radius $9''$ and width $3''$ by using the PHOT task in the IRAF APPHOT package and the obtained sky value was subtracted.

We next made azimuthally averaged radial surface brightness profiles in both blue and red images with a radial sampling of $0''.1$. In each galaxy these profiles are made along the ellipses fitted with a fixed position angle to the isophotes of the galaxy images in the red band (the position angles are taken from Table 2 by Smail et al. 1997). Thus the

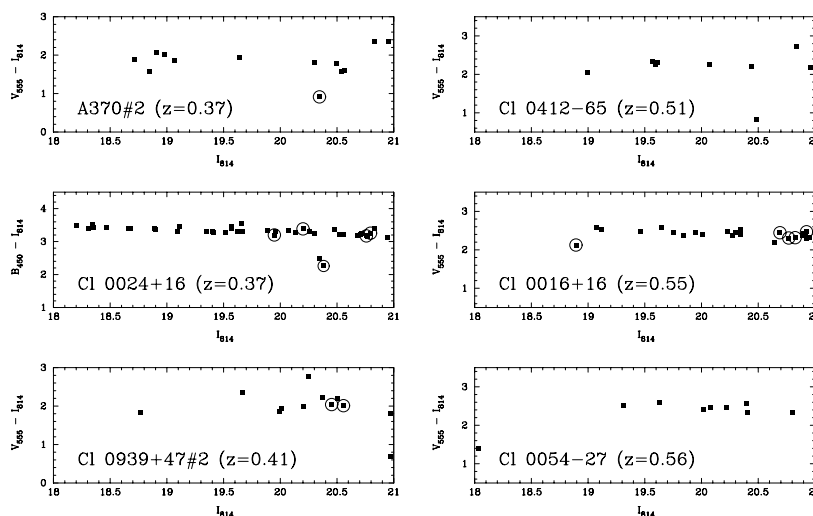


FIG. 1.—Color-magnitude diagrams for the sample galaxies in the clusters. Squares in circles indicate objects whose color gradients cannot be obtained because of a low S/N or because of a position close to an edge of the image. The label “#2” after the cluster name indicates the outer field of the cluster.

¹ See <http://star-www.dur.ac.uk/~irs/morphs.html>.

surface brightness profiles in the two bands are derived based on the same fitted elliptical isophotes. In Figure 2, representative surface brightness profiles of our sample galaxies are shown. The profiles of the brightest, intermediate, and faintest sample galaxies in each cluster are shown in top, middle, and bottom panels, respectively. The profiles of almost all the galaxies in our sample are well described by the $r^{1/4}$ law. To derive color profiles, the surface brightness profile in the red band is subtracted from the profile in the blue band. Figure 3 shows the resulting color profiles with the same arrangement as in Figure 2. An error bar for each

data point includes photometric error, local sky subtraction error (1% of the sky value around each object is adopted), and dispersion of colors along each elliptical isophote. It is important to describe here the two-dimensional color distribution in the sample galaxies. The color maps were constructed by dividing the blue image by the red image after adjusting the positional displacement and difference of sizes in the PSFs. Almost all the color maps show smooth color distribution and do not show any asymmetric or peculiar features. Thus the color profiles well represent the color distribution in each galaxy.

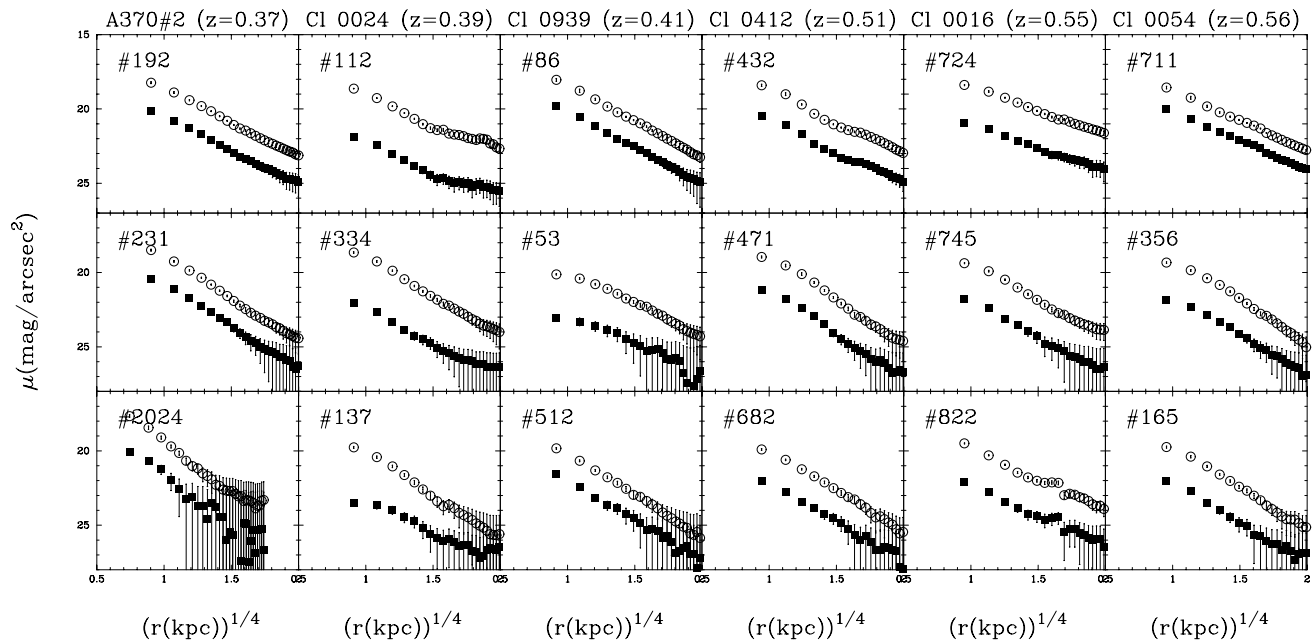


FIG. 2.—Azimuthally averaged radial surface brightness profiles of representative galaxies in the sample for the brightest (*top*), intermediate (*middle*), and faintest (*bottom*) sample galaxies in each cluster, showing the profile in a blue band (*squares*) and in a red band (*circles*). Galaxies are identified at upper left in each panel.

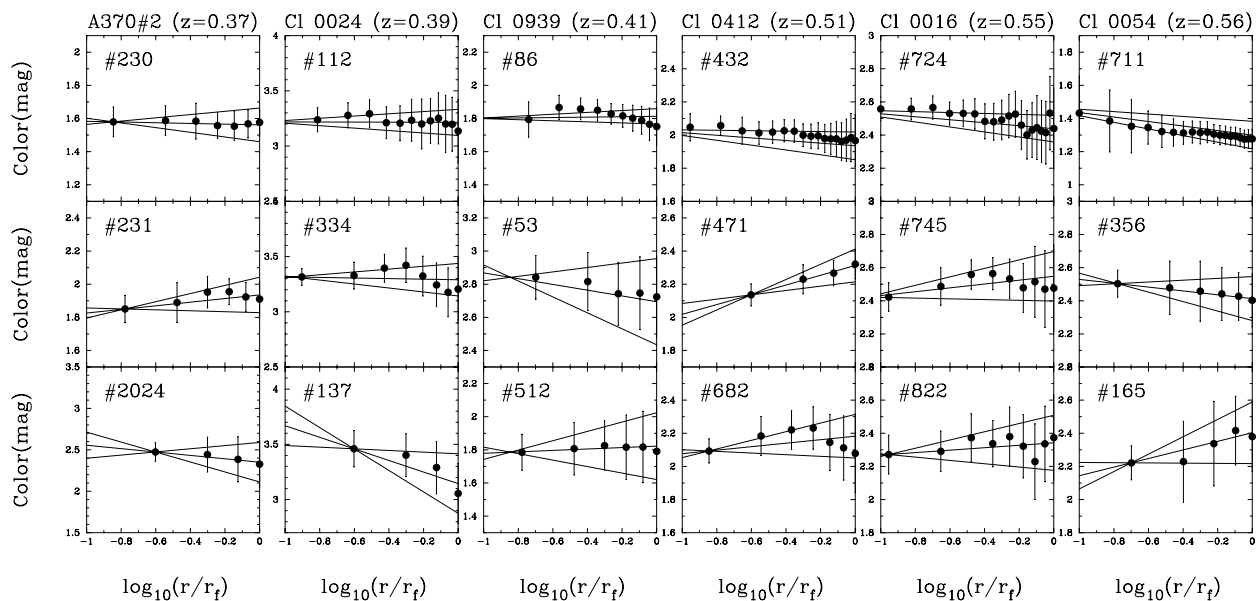


FIG. 3.—Color profiles and fitted slopes of the representative galaxies. Galaxies and their arrangement are the same as in Fig. 2. The middle line in each panel shows the best-fit slope. The other two lines show the slopes with $\pm 1\sigma$ of the best fit. Abscissas refer to the logarithm of the radius normalized by the outermost radius, r_r , used for fitting each color profile.

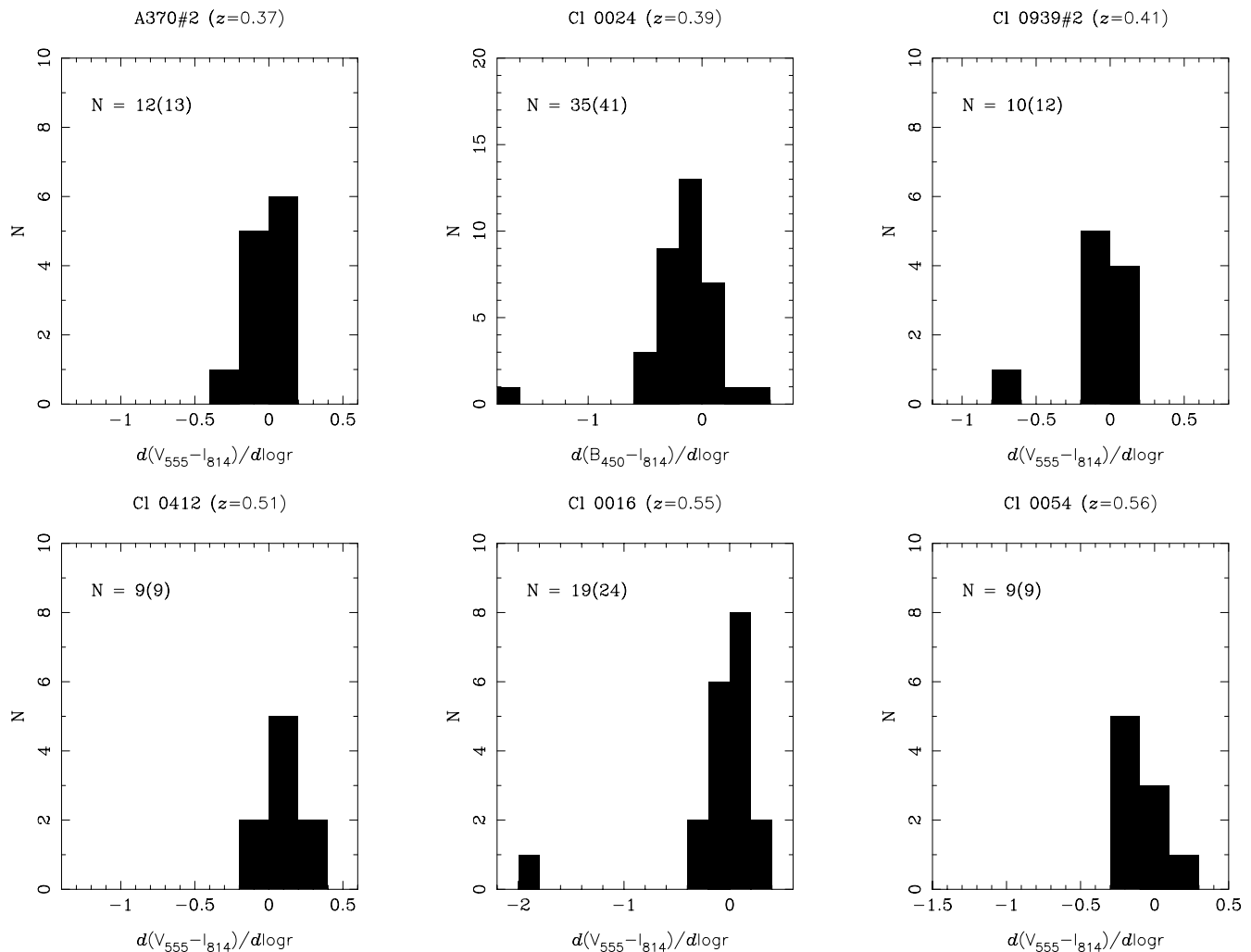


FIG. 4.— Histograms of the color gradients in the sample galaxies in each sample cluster. The total number of objects in each histogram is shown at upper left in each panel, and the number in parentheses indicates the total number of sample galaxies in each cluster. Each cluster and its redshift are shown above each panel.

Finally, slopes of the color profiles, i.e., color gradients, in the sample galaxies are derived by least-square fitting within effective radii obtained from the surface brightness profiles in the red band, assuming the $r^{1/4}$ law. Fitting for the color gradients is done after removing data points with errors larger than 0.3 mag. We do not derive the gradients of the profiles with fewer than three accepted data points. The average number of the data points used for the fitting is about eight and the rejected objects are minor. The resulting color gradients for the sample galaxies are listed with the 1σ fitting errors in Tables 2–7. Figure 3 indicates resulting slopes of the color gradients, as well as the slopes with $\pm 1\sigma$. In this figure, abscissas refer to the logarithm of the radius normalized by the outermost radius, r_f , used for fitting each color profile. For most of the sample galaxies, r_f is roughly equal to r_e .

Figure 4 shows a histogram for the color gradients of the sample galaxies in each cluster. Each bin of the histograms is 0.2 mag dex^{-1} , comparable to the average fitting error. It is found that the distributions of the gradients are very narrow except for a few outliers, namely, Nos. 535 and 738 in CL 0024+16, 2005 in CL 0939+47, and 2050 in CL 0016+16. The first three are significantly out of the C-M

relation toward the blue side, but the last one is almost on the relation. Since the range of the distribution of the color gradients is comparable to or only slightly larger than the estimated error for the slopes, the intrinsic dispersions of the color gradients must be considerably small. (The dispersion of the color gradients in nearby elliptical galaxies is about $0.04 \text{ mag dex}^{-1}$; Peletier et al. 1990a; Paper I.) It is intriguing that the color gradients of elliptical galaxies are uniform even at intermediate redshift. Furthermore, this encourages the comparison between model gradients and observed gradients in distant clusters, despite rather large errors for the observed slopes.

4. ORIGIN OF COLOR GRADIENTS IN CLUSTER ELLIPTICAL GALAXIES

4.1. Models

To examine whether the origin of color gradients is the stellar metallicity or the age, we adopt the same approach as in Paper I, and the reader should refer to it in detail. We briefly summarize it here. An observed color gradient can be reproduced by either a metallicity gradient or an age gradient of stellar populations in an elliptical galaxy at

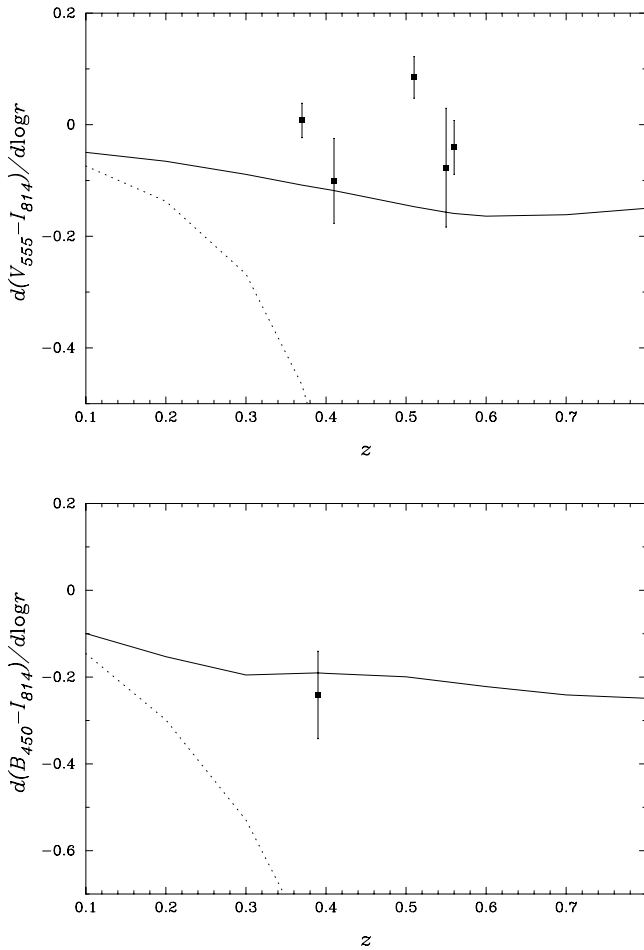


FIG. 5.—The mean color gradient for each cluster versus redshift, representing the evolutionary track of the color gradient caused by the metallicity gradient (*solid curve*) and the track caused by the age gradient (*dotted curve*; see text for details).

$z = 0$. However, since the color gradient caused by a metallicity gradient is expected to follow a different evolution from that caused by an age gradient, the origin of the color gradients can be found by comparing the observed ones at high redshift with those predicted by model. For this purpose, using the population synthesis model (Kodama & Arimoto 1997; Kobayashi, Tsujimoto, & Nomoto 2000), we construct two model galaxies; in one (hereafter the metallicity-gradient model) the color gradient is made by

the pure metallicity gradient without an age gradient, and in the other (hereafter the age-gradient model) the color gradient is made by the pure age gradient without a metallicity gradient. In the metallicity-gradient model, the metallicity gradient is produced by assuming that a galactic wind blew later in the inner region in an elliptical galaxy; star formation continued longer, and thus the mean stellar metallicity became higher at the inner region. For the age-gradient model, star formation started earlier in the inner region and thus the mean age of stellar populations is older than those in the outer region. The stellar population in each region in an elliptical galaxy is assumed to be made by a single burst and to evolve independently of other regions. The model parameters used here are the same as those in Paper I, which are chosen to reproduce the typical color gradient at $z = 0$. The mean value of $\Delta(B-R)/\Delta \log r$ of $-0.09 \text{ mag dex}^{-1}$ obtained by Peletier et al. (1990a) is adopted as the typical color gradient at $z = 0$. Note that these model galaxies must be old (8–15 Gyr) to reproduce colors in nearby elliptical galaxies. Then we calculate the spectral evolution in each region of the model galaxies and their color gradients at any redshifts using the response functions including each filter on the *HST*. It should be emphasized that we do not intend to study physical formation process of elliptical galaxies in this paper, but we aim to depict the evolution of the color gradient caused by either the metallicity gradient or the age gradient in comparison with the observed ones. The actual physical process that caused the metallicity or age gradient may be different from our brief ideas presented in the model description. However, it is not a problem here, because once such a gradient is formed, subsequent evolution of the stellar population is unique and does not depend on the formation process.

The two curves in each panel of Figure 5 show the evolutionary track of the model color gradients; the solid curve indicates the evolution for the metallicity-gradient model, and the dotted curve, that for the age-gradient model. The model color gradient predicted by the metallicity gradient is almost constant at redshift less than $z \sim 1$, while that by the age gradient changes abruptly and shows quite a steep gradient even at $z = 0.3$. We will compare the model gradients with the observed ones in the next subsection.

4.2. Model versus Observation

The mean values of the color gradients in each cluster sample are plotted against redshift in Figure 5. Error bars indicate the mean error of the gradients in each cluster.

TABLE 1
SAMPLE CLUSTERS

OBJECT	z	IMAGE CENTER		EXPOSURE (s)	
		α (J2000.0)	δ (J2000.0)	F555W ^a	F814W
A370 Field 2	0.37	02 40 01.1	−01 36 45	8000	12600
CL 0024+16	0.39	00 26 35.6	+17 09 43	23400	13200
CL 0939+47 Field 2	0.41	09 43 02.5	+46 56 07	4000	6300
CL 0412−65	0.51	04 12 51.7	−65 50 17	12600	14700
CL 0016+16	0.55	00 18 33.6	+16 25 46	12600	16800
CL 0054−27	0.56	00 56 54.6	−27 40 31	12600	16800

NOTE.—Units of right ascension are hours, minutes, and seconds, and units of declination are degrees, arcminutes, and arcseconds.

^a For CL 0024+16, the exposure time in the F450W band image.

TABLE 2
SAMPLE GALAXIES (A370)

Object	I_{814} (mag)	$V_{555}-I_{814}$ (mag)	$\Delta(V_{555}-I_{814})/\Delta \log r$ (mag dex $^{-1}$)	N^a
192	18.712	1.897	0.11 ± 0.06	16
221	20.828	2.345	0.11 ± 0.39	4
230	18.847	1.578	-0.02 ± 0.12	7
231	19.641	1.926	0.11 ± 0.14	6
232	18.911	2.067	-0.08 ± 0.12	8
265	20.491	1.786	-0.09 ± 0.20	6
289	20.539	1.575	0.17 ± 0.16	5
351	20.562	1.602	-0.08 ± 0.11	9
377	18.977	2.021	-0.04 ± 0.08	17
458	20.299	1.817	0.11 ± 0.29	6
469	20.346	0.915
487	19.071	1.867	0.00 ± 0.08	16
2024	20.955	2.343	-0.21 ± 0.40	4

^a Number of data points in a color profile for deriving a color gradient.

TABLE 3
SAMPLE GALAXIES (CL 0024 + 16)

Object	I_{814} (mag)	$B_{450}-I_{814}$ (mag)	$\Delta(B_{450}-I_{814})/\Delta \log r$ (mag dex $^{-1}$)	N
89	19.947	3.199
112	19.519	3.278	-0.00 ± 0.11	13
113	18.892	3.404	-0.13 ± 0.09	14
137	20.827	3.391	-0.52 ± 0.45	4
145	20.717	3.251	0.18 ± 0.38	4
147	19.411	3.290	-0.27 ± 0.12	10
169	20.795	3.255
179	19.654	3.559	-0.01 ± 0.18	7
261	19.623	3.310	0.06 ± 0.23	7
268	19.400	3.296	0.14 ± 0.19	8
280	18.200	3.481	-0.22 ± 0.06	30
294	19.959	3.296	0.42 ± 0.21	6
304	18.469	3.419	-0.28 ± 0.06	26
327	20.759	3.173
334	19.567	3.389	-0.03 ± 0.15	8
337	20.069	3.348	0.16 ± 0.37	4
342	18.680	3.412	-0.05 ± 0.08	20
343	18.348	3.506	-0.28 ± 0.05	30
353	20.557	3.220	0.01 ± 0.40	4
362	18.901	3.367	-0.04 ± 0.12	8
365	18.309	3.403	-0.17 ± 0.06	27
403	19.349	3.317	-0.55 ± 0.14	11
419	19.573	3.444	-0.13 ± 0.19	7
479	20.768	3.170	0.14 ± 0.39	4
514	19.883	3.325	-0.34 ± 0.19	7
521	20.259	3.318	0.22 ± 0.29	5
535	20.343	2.501	-1.68 ± 0.12	17
573	18.353	3.424	-0.19 ± 0.20	10
590	20.201	3.385
621	18.660	3.405	-0.20 ± 0.07	16
653	19.090	3.311	-0.44 ± 0.12	10
669	20.130	3.282	-0.38 ± 0.24	6
675	20.709	3.216	-0.07 ± 0.37	4
678	20.298	3.256	-0.15 ± 0.30	5
685	20.683	3.196	-0.30 ± 0.38	4
738	20.522	3.208	-3.23 ± 0.35	10
796	19.109	3.450	-0.22 ± 0.11	13
876	19.669	3.315	-0.15 ± 0.23	5
934	20.382	2.259
3006	20.944	3.118	0.13 ± 0.14	18
3012	20.475	3.367	-0.12 ± 0.15	12

TABLE 4
SAMPLE GALAXIES (CL 0939 + 47)

Object	I_{814} (mag)	$V_{450}-I_{814}$ (mag)	$\Delta(V_{450}-I_{814})/\Delta \log r$ (mag dex $^{-1}$)	N
31	20.452	2.040
53	20.247	2.770	-0.17 ± 0.31	5
86	18.769	1.822	0.01 ± 0.04	11
270	19.993	1.866	-0.18 ± 0.12	10
337	20.507	2.209	0.02 ± 0.20	6
404	19.670	2.344	-0.01 ± 0.19	7
426	20.014	1.947	-0.10 ± 0.15	7
429	20.372	2.211	0.18 ± 0.31	5
512	20.972	1.817	0.04 ± 0.24	6
515	20.208	1.997	-0.04 ± 0.13	9
566	20.557	2.010
2005	20.968	0.700	-0.76 ± 0.31	11

Clearly, the figure favors the metallicity gradient much more than the age gradient as the origin of the color gradients. This result does not depend on cosmological parameters or parameters for an evolutionary model of a galaxy within a reasonable range and does not change even if we consider the dispersion of the color gradients in the sample galaxies (see Fig. 4) or in nearby elliptical galaxies (~ 0.04 mag dex $^{-1}$). Although the sample galaxies for which membership in the clusters are spectroscopically confirmed are few (Dressler et al. 1999), background or foreground contaminations are not expected to affect the result for the origin of the color gradients because the result does not change even if we remove galaxies that deviate significantly from the C-M relation in each cluster. The color gradients in several sample galaxies may be affected by other galaxies close to them, and the color profile of a galaxy located close to an edge of the chip or on a joint between the cameras may be somewhat spurious. However, our result holds even after removing galaxies that may suffer from these effects.

Considering the result in Paper I, in both cluster and field the primary origin of the color gradients in elliptical galaxies is considered to be the stellar metallicity. However, it is interesting to point out that the mean values of the color gradients seem to deviate upward from the line for the metallicity-gradient model. Our models are calibrated by the color gradients seen in nearby elliptical galaxies by Peltier et al. (1990a), in which most of the sample elliptical galaxies are found in a field or group environment. Therefore, the upward deviation might indicate a different environmental effect on the color gradients of elliptical gal-

TABLE 5
SAMPLE GALAXIES (CL 0412 - 65)

Object	I_{814} (mag)	$V_{450}-I_{814}$ (mag)	$\Delta(V_{450}-I_{814})/\Delta \log r$ (mag dex $^{-1}$)	N
431	20.835	2.715	0.03 ± 0.22	7
432	18.992	2.044	-0.08 ± 0.07	18
471	20.074	2.254	0.29 ± 0.16	4
472	19.571	2.330	0.11 ± 0.10	9
635	19.612	2.300	0.06 ± 0.10	14
657	19.597	2.265	0.06 ± 0.10	7
682	20.960	2.183	0.11 ± 0.16	7
695	20.440	2.213	-0.04 ± 0.16	4
772	20.489	0.839	0.23 ± 0.06	14

TABLE 6
SAMPLE GALAXIES (CL 0016+16)

Object	I_{814} (mag)	$V_{555}-I_{814}$ (mag)	$\Delta(V_{555}-I_{814})/\Delta \log r$ (mag dex $^{-1}$)	N
271	20.913	2.387	0.29 ± 0.23	4
438	19.754	2.460	-0.32 ± 0.07	19
461	20.296	2.461	0.19 ± 0.23	4
531	20.692	2.443
602	20.926	2.469
606	20.769	2.305
611	20.232	2.466	0.19 ± 0.16	8
612	19.648	2.574	-0.12 ± 0.10	10
650	19.464	2.482	-0.05 ± 0.07	17
653	19.837	2.384	-0.00 ± 0.13	8
659	19.950	2.441	0.04 ± 0.13	10
724	19.075	2.582	-0.09 ± 0.06	20
725	19.117	2.531	-0.02 ± 0.05	28
726	20.826	2.317
732	20.009	2.398	0.26 ± 0.18	7
745	20.342	2.519	0.12 ± 0.14	9
802	20.898	2.411	0.06 ± 0.18	7
822	20.956	2.320	0.07 ± 0.17	9
823	20.346	2.387	-0.06 ± 0.12	10
843	20.270	2.372	0.08 ± 0.12	7
903	20.927	2.300	0.14 ± 0.27	4
2026	20.643	2.187	-0.32 ± 0.19	5
2050	20.894	2.366	-1.92 ± 0.42	4
3002	18.894	2.122

TABLE 7
SAMPLE GALAXIES (CL 0054-27)

Object	I_{814} (mag)	$V_{555}-I_{814}$ (mag)	$\Delta(V_{555}-I_{814})/\Delta \log r$ (mag dex $^{-1}$)	N
165	20.802	2.329	0.25 ± 0.27	5
191	20.225	2.459	-0.11 ± 0.15	9
216	19.627	2.600	-0.01 ± 0.12	9
229	20.393	2.565	0.07 ± 0.20	5
356	20.080	2.469	-0.12 ± 0.17	6
365	20.407	2.345	0.06 ± 0.17	7
440	19.316	2.514	-0.12 ± 0.11	13
529	20.021	2.415	-0.26 ± 0.12	10
711	18.037	1.403	-0.14 ± 0.06	20

axies in rich clusters and those in the field. However, the correlation between the mean value and the degree of the concentration in each cluster is not seen. In addition, the mean gradients of the clusters for which outer field images were taken do not show larger values than others. Further detailed study on the color gradients in cluster elliptical galaxies and field ones at $z = 0$, as well as at high redshift, should be done.

We would like to thank C. Kobayashi, N. Arimoto, and T. Kodama for fruitful collaboration in Paper I. This work was financially supported in part by grant 11740123 from the Ministry of Education, Science, Sports and Culture of Japan.

REFERENCES

- Arimoto, N. 1996, in ASP Conf. Ser. 98, From Stars to Galaxies, ed. C. Leitherer, U. Fritze-von Alvensleben, & J. Huchra (San Francisco: ASP), 287
- Barger, A., Cowie, L. L., Trentham, N., Fulton, E., Hu, E. M., Songaila, A., & Hall, D. 1999, *AJ*, 117, 102
- Baugh, C. M., Cole, S., & Frenk, C. S. 1996, *MNRAS*, 283, 1361
- Bregman, J. N., Snider, B. A., Grego, R., & Cox, C. V. 1998, *ApJ*, 499, 670
- Carollo, C. M., Danziger, I. J., & Buson, L. 1993, *MNRAS*, 265, 553
- Davies, R. L., Sadler, E. M., & Peletier, R. F. 1993, *MNRAS*, 262, 650
- Dressler, A., et al. 1997, *ApJ*, 490, 577
- Dressler, A., Smail, I., Poggianti, B. M., Butcher H., Couch, W. J., Ellis, R. S., & Oemler, A., Jr. 1999, *ApJS*, 122, 51
- Franx, M., Illingworth, G., & Heckman, T. 1989, *AJ*, 98, 538
- Gonzalez, J. J. 1993, Ph.D. thesis, Univ. California
- Goudfrooij, P., & de Jong, T. 1995, *A&A*, 298, 784
- Goudfrooij, P., Hansen, L., Jørgensen, H. E., Nørgaard-Nielsen, H. U., de Jong, T., & van den Hoek, L. B. 1994, *A&AS*, 104, 179
- Kobayashi, C., & Arimoto, N. 1999, *ApJ*, 527, 573
- Kobayashi, C., Tsujimoto, T., & Nomoto, K. 2000, *ApJ*, in press
- Kodama, T., & Arimoto, N. 1997, *A&A*, 320, 41
- Kodama, T., Arimoto, N., Barger, A. J., & Aragón-Salamanca, A. 1998a, *A&A*, 334, 99
- Kodama, T., Bower, R. G., & Bell, E. F. 1998b, *MNRAS*, 306, 561
- Krist, J. E. 1995, in ASP Conf. Ser. 77, Astronomical Data Analysis Software and Systems IV, ed. R. A. Shaw, H. E. Payne, & J. M. E. Hayes (San Francisco: ASP), 349
- Krist, J. E., & Hook, R. 1997, *The Tiny Tim User's Guide* (version 4.4; Baltimore: STScI)
- Michard, R. 1999, *A&AS*, 137, 245
- Peletier, R. F., Davies, R. L., Illingworth, G. D., Davis, L. E., & Cawson, M. 1990a, *AJ*, 100, 1091
- Peletier, R. F., Valentijn, E. A., & Jameson, R. F. 1990b, *A&A*, 233, 62
- Silva, D. R., & Wise, M. W. 1996, *ApJ*, 457, L15
- Smail, I., Dressler, A., Couch, W. J., Ellis, R. S., Oemler, A., Jr., Butcher, H., & Sharples, R. 1997, *ApJS*, 110, 213
- Stanford, S. A., Eisenhardt, P. R., & Dickinson, M. 1998, *ApJ*, 492, 461
- Tamura, N., Kobayashi, C., Arimoto, N., Kodama, T., & Ohta, K. 2000, *AJ*, 119, 2134 (Paper I)
- Vader, J. P., Vigroux, L., Lachièze-Rey, M., & Souviron, J. 1988, *A&A*, 203, 217
- Williams, R. E., et al. 1996, *AJ*, 112, 1335
- Wise, M. W., & Silva, D. R. 1996, *ApJ*, 461, 155
- Worthey, G., Trager, S. C., & Faber, S. M. 1996, in ASP Conf. Ser. 86, Fresh Views of Elliptical Galaxies, ed. A. Buzzoni, A. Renzini, & A. Serrano (San Francisco: ASP), 203